Low-dose cadmium potentiates lung inflammatory response to 2009 pandemic H1N1 influenza virus in mice

Joshua D. Chandler[*], Xin Hu[*], Eunju Ko[†], Soojin Park[†], Jolyn Fernandes[*], Young-Tae Lee[†], Michael L. Orr[*], Li Hao[*], M. Ryan Smith[*], David C. Neujahr[*], Karan Uppal[*], Sang-Moo Kang[†], Dean P. Jones[*‡] and Young-Mi Go[*‡]

[*] Division of Pulmonary, Allergy and Critical Care Medicine, Emory University School of Medicine, Atlanta, GA, 30322, [†] Center for Inflammation, Immunity and Infection, Georgia State University, Atlanta, GA, 30303.

Running Head: Cadmium potentiates H1N1 lung inflammation in mice

[‡] Corresponding author: Whitehead Biomedical Research Building, 615 Michael St, Room 225 Atlanta, GA, 30322. Phone: 404-727-5984. Fax: 404-727-2974. E-mail: dpjones@emory.edu

Acknowledgements

Dr. Young-Mi Go and Dr. Dean P. Jones share equal senior authorship in this collaborative research. We thank the Emory Integrated Genomics Core, Dana B. Barr PhD and Priya E. D'Souza MPH for technical assistance. This study was supported by NIEHS Grant R01 ES023485 (DPJ and YMG), R21 ES025632 (DPJ and YMG), NIH S10 OD018006 (DPJ), NIH/NIAID grants R01 AI105170 (SMK), R01 AI093772 (SMK), and R21 AI119366 (SMK), and NHLBI F32 1F32HL132493 (JDC) and Cystic Fibrosis Foundation CHANDL16F0 (JDC).

25 **Author Contributions**

26 - Designed research – YMG, DPJ, SMK
27 - Performed research – JDC, JF, XH, YTL, EJK, SJP, DCN, MRS, MLO, LH
28 - Contributed new reagents or analytic tools – KU
29 - Analyzed data – JDC, YTL, SJP, EJK, JF, XH, MRS
30 - Wrote the paper – JDC, YMG, DPJ

31

32 **Declaration of Competing Financial Interests**

33 The authors declare they have no actual or potential competing financial interests.

34

35 **Abbreviations**

36 Cd, Cadmium; Ctl, control; Cys, cysteine; CySS, cystine; FACS, fluorescence-activated cell
37 sorting; FDR, False discovery rate; GSEA, Gene set enrichment analysis; H1N1, pandemic 2009
38 influenza A (H1N1) virus; HRM, High resolution metabolomics; ICP-MS, Inductively coupled
39 plasma mass spectrometer; interferon gamma, IFNγ; interleukin-1beta, IL-1β; LC, liquid
40 chromatograph; MS, mass spectrometer; *m/z*, mass to charge; RT, retention time; sPLS, sparse
41 partial least squares; Trx, thioredoxin.

42

43

44

45

46

47

48

Abstract

BACKGROUND: Cadmium (Cd) is a toxic, pro-inflammatory metal ubiquitous in the diet that accumulates in body organs due to inefficient elimination. Many individuals exposed to dietary Cd are also infected by seasonal influenza virus. The H1N1 strain causes mild to severe pneumonia which can be fatal.

OBJECTIVES: To determine the influence of low-dose Cd exposure on inflammatory responses to H1N1 influenza A virus.

METHODS: We exposed mice to low-dose (1 mg $CdCl_2$/l) Cd or vehicle (water) for 16 weeks prior to infection with a sub-lethal dose of H1N1. Lung inflammation was assessed by histopathology and flow cytometry. We used a combination of transcriptomics, metabolomics and bioinformatics to determine the molecular associations of inflammatory cells important in Cd-exacerbated responses.

RESULTS: Cd-treated mice had increased lung tissue inflammatory cells, including neutrophils, monocytes, T lymphocytes and dendritic cells, following H1N1 infection. Lung genetic responses to infection (increasing TNF-α, interferon and complement, and decreasing myogenesis) were also exacerbated. Global correlations with immune cell counts, leading edge gene transcripts and metabolites revealed that Cd increased correlation of myeloid immune cells with pro-inflammatory genes, particularly interferon-γ, and metabolites in amino acid, nucleobase, glycerophospholipid and vitamin B3 pathways.

DISCUSSION: Cd burden in mice increased inflammation in response to sub-lethal H1N1 challenge, which was coordinated by genetic and metabolic responses, and could provide new targets for intervention against lethal inflammatory pathology of clinical H1N1 infection.

Keywords: Environmental safety, exposome, heavy metals, influenza A virus, public health.

73 **Introduction**

74 Recent studies of the environmental toxic metal cadmium (Cd) show that levels found in
75 human lungs potentiate pro-inflammatory signaling by the redox-sensitive transcription factor
76 NF-κB (Chandler et al. 2016b; Olszowski et al. 2012). Cd is a commercially important metal
77 used in NiCd batteries, plating, pigments and plastics (Kataranovski et al. 2009; Waalkes 2003;
78 Zhang et al. 2014). Earlier occupational toxicities from Cd have been largely eliminated by
79 occupational hygiene, and tobacco use remains as a major avoidable source of exposure. In non-
80 smokers, diet is the most important source of human Cd burden, on average representing about
81 half of the exposure of individuals with active tobacco use (Riederer et al. 2013; Satarug and
82 Moore 2004). Although Cd is poorly absorbed, there is no effective mechanism for elimination
83 so that the biological half-life in humans is over 10 years (Satarug and Moore 2004; Suwazono et
84 al. 2009). Our mechanistic studies show that low concentrations of Cd cause oxidation of
85 thiol/disulfide redox systems (Go et al. 2011; Go et al. 2013a; Go et al. 2014), disrupt the actin-
86 cytoskeleton regulation (Go et al. 2013a), cause translocation of thioredoxin-1 (Trx1) into the
87 nucleus (Go et al. 2013a), increase NF-κB activity and increase pro-inflammatory cytokines (Go
88 et al. 2011; Go et al. 2013b). Cd causes a dose-dependent oxidation of plasma cysteine/cystine
89 (Cys/CySS) redox state (E_h CySS, Y.-M. Go, unpublished), the major low molecular weight
90 thiol/disulfide system in plasma previously associated with pro-inflammatory signaling (Go and
91 Jones 2005, 2011). Additionally, studies with a transgenic NLS-thioredoxin-1 (Trx1) mouse
92 showed that increased nuclear Trx1 substantially potentiated adverse outcomes from H1N1
93 influenza infection (Go et al. 2011) and also increased oxidation of thiol/disulfide redox systems
94 (Go et al. 2011).

95 H1N1 and other influenza A strains are highly infectious (Liu et al. 2015; Xing et al.
96 2015) and cause variable severity of disease (Baigent and McCauley 2003a, b; Safronetz et al.

97 2011a, b; Taubenberger and Kash 2010a, b). Host genetics impact severity of response (Horby et
98 al. 2012, 2013), but inter-individual differences in sensitivity have mainly been linked to
99 demographic factors, such as age and general health (Gagnon et al. 2013; Wilson et al. 2014). In
100 most cases, the pandemic 2009 influenza A (H1N1) virus caused an uncomplicated respiratory
101 tract illness with symptoms similar to those caused by seasonal influenza viruses. However,
102 severe responses also occurred in a fraction of patients and were linked to increased levels of
103 pro-inflammatory cytokines, termed a "cytokine storm" (Gautam 2012; Liu et al. 2016), as well
104 as to excess activity of the complement system (Monsalvo et al. 2011). Cytokine storm included
105 high levels of IL-6 and was strongly associated with decreased lung function and death
106 (Bermejo-Martin et al. 2009; To et al. 2010).
107 The current study was designed to test whether Cd burden, at a level found in lungs of
108 non-smokers, enhanced severity of HIN1 influenza virus infection in a mouse model. Mice were
109 given water ad libitum with or without $CdCl_2$ (1 mg/l) for 16 weeks, and 10 days before sacrifice
110 each mouse was also intranasally exposed to either sub-lethal H1N1 or mock (sterile saline)
111 treatment. Lung histopathology and immune cell counts were used to evaluate inflammatory
112 responses and pathology. Gene expression analysis and high-resolution metabolomics were used
113 to identify Cd-dependent associations of inflammatory cells using the open-source software,
114 *xMWAS* (Uppal et al. 2018). Targeted analysis of IFNγ protein correlations with immune cells
115 was used to confirm *xMWAS* results.
116
117
118
119
120

121 **Materials and Methods**

122

123 **Animals**

124 All experimental protocols for animal studies were approved by Emory University and Georgia
125 State University Internal Care and Use Committees. Experimental methods were carried out in
126 accordance with the relevant guidelines and regulations. Male C57BL6 mice (n = 11-13 per
127 group) aged 8 weeks (Jackson Labs, Bar Harbor, ME, USA) were maintained in clean facilities
128 and given sterile-filtered drinking water with 1 mg/l $CdCl_2$ (Sigma-Aldrich, St. Louis, MO,
129 USA) or vehicle for 16 weeks (including the 10-day duration of H1N1 infection). Food content
130 of Cd (62 ± 1 ng/g food) was negligible compared to the Cd derived from water (Chandler et al.
131 2016b). Ten days prior to study completion, mice were inoculated with H1N1
132 (A/California/04/2009; dose of 0.6 x 10^3 pfu) under isoflurane anesthesia. Day 10 was chosen as
133 the time point of maximal sub-lethal morbidity but also as a clinically relevant time point for
134 severe and persistent cases. People infected with influenza are generally asymptomatic for 1-4
135 days, then exhibit symptoms for 3-7 days
136 (https://www.cdc.gov/flu/professionals/acip/clinical.htm). Virus titer from mouse lung
137 homogenate is expressed as the $\log_{10}$ of the 50% egg infective dose (EID_{50}) per ml homogenate.
138 For the main study, mice were weighed every 7 days until infection, then daily for the
139 remaining 10 days. Mice were observed daily for other signs of influenza morbidity, e.g., a
140 ruffled hair coat or labored breathing, and no apparent differences were observed between H1N1
141 and Cd+H1N1. Airway reactivity as measured by airway enhanced pause (PenH) was used to
142 evaluate possible airway effects (Chandler et al. 2016a; Hwang et al. 2016). The PenH
143 procedure does not require additional compound exposures (e.g., methacholine) which could
144 impact the lung metabolome.

145

146 **Cd measurement by Inductively-Coupled Plasma Mass Spectrometry (ICP-MS)**

147 Lung tissue ^{114}Cd was assayed as previously described (Chandler et al. 2016b). ICP-MS
148 procedures conformed to accuracy (100 ± 10%) and precision standards (relative standard
149 deviation < 12%). Cd values were normalized to tissue mass. Human lung tissue samples were
150 collected in the Emory Transplant Center (Emory IRB protocol 000006248) and maintained
151 frozen at -80 ˚C until analysis.

152

153 **Flow cytometry and staining**

154 Immune cells in lung tissue were quantified by fluorescence-activated cell sorting (FACS). Lung
155 tissues were homogenized in DMEM and applied to Percoll gradients before washing with PBS.
156 Total viable cells were counted using a hemocytometer with 0.4% trypan blue for dye exclusion.
157 A subset of cells for FACS analysis was treated with anti-surface marker antibodies including
158 CD11b (M1/70), CD45 (30-F11), B220 (RA3-6B2), Siglec F (E50-2440) (BD Pharmingen,
159 Franklin Lakes, NJ, USA); CD11c (N418), F4/80 (BM8) (eBioscience, Thermo Fisher Scientific,
160 Waltham, MA, USA); and CD103 (2E7), Ly6c (HK1.4), MHC-II (M5/114.15.2), CD3 (17A2),
161 CD4 (GK1.5), and CD8 (53-5.8) (BioLegend, San Diego, CA, USA). Data were acquired using
162 an LSR-II/Fortessa (Becton-Dickinson, Franklin Lakes, NJ, USA) and analyzed using FlowJo v.
163 10.1 (Tree Star, Inc., Ashland, OR, USA). CD11b^{+} DCs were gated as those with low CD103
164 expression, and vice-versa; we did not analyze a mixed population (CD11b^{+}/CD103^{+}). Absolute
165 counts were expressed from the percentage from FACS analysis multiplied by viable cell counts
166 obtained with a hemocytometer.

167

168

169 **Cytokine and chemokine assays**

170 IFNγ was measured as previously described (Ko et al. 2016; Lee et al. 2015; Lee et al. 2016).
171 Briefly, right lung lobe extracts were prepared by grinding and filter straining prior to IFNγ
172 measurement according to manufacturer instructions (eBioscience, Thermo Fisher Scientific,
173 Waltham, MA, USA).

174

175 **Analysis of glutathione and cysteine**

176 Glutathione (GSH), oxidized glutathione (GSSG), cysteine (Cys) and oxidized form of Cys
177 (cystine, CySS) in lung tissue and plasma were analyzed by HPLC with fluorescence detection
178 (Go and Jones 2005; Jones et al. 2002; Jones and Liang 2009). Protein assay (bicinchonicic acid)
179 was used to standardize the results to intracellular concentrations. Redox states of GSH/GSSG
180 (E_h[GSSG]) and Cys/CySS (E_h[CySS]) were calculated using the Nernst equation (Go and Jones
181 2005; Jones et al. 2002; Jones and Liang 2009).

182

183 **Histopathology**

184 The lung collected at 10 days after challenge was fixed with 10% normal buffered formalin
185 (NBF) in PBS. After fixation NBF tissues were transferred to 70% alcohol and processed to
186 paraffin using a Shandon Excelsior AS (Thermo Fisher Scientific). A standard program of
187 dehydration was carried out in ethanol 70%, 80%, 90%, 95%, 100%, 100% 1 hour each,
188 followed by xylenes twice for 30 min each. Finally, the tissue was soaked in paraffin for 30 min
189 and repeated once, then held in the second paraffin bath for 1 hour. Left lung tissue sections (4
190 mice per group) were stained with hematoxylin and eosin (H&E) to assess histopathological
191 changes as described (Ko et al. 2016). Images were acquired by Axiovert 100 (Zeiss,

192 Oberkochen, Germany) at 100X magnification, and inflammation was blindly scored as
193 previously described (Ko et al. 2016).
194
195 **Transcriptomics**
196 20-25 mg of lung tissue was stored in RNAlater (Qiagen, Hilden, Germany) at -80 ˚C prior to
197 lysis and RNA isolation using the miRNEasy kit (Qiagen, Hilden, Germany). 250 ng of RNA
198 was prepared and hybridized to MoGene ST 2.0 arrays (Affymetrix, Thermo Fisher Scientific,
199 Waltham, MA, USA). CEL files were converted to a Robust-Multi Array (RMA) and loaded in
200 the gene set enrichment analysis (GSEA) Java applet (v. 2.2; Broad Institute) to test gene set
201 enrichment. Annotations were made using MSigDB file 'MoGene_2_0_st.chip', accessed from
202 the GSEA applet. Redundant annotations were collapsed using maximum intensities.
203
204 **High resolution metabolomics (HRM)**
205 Lung tissue metabolites were extracted from 20-30 mg tissue in 15 µl/mg of 2:1
206 acetonitrile:water containing internal standards per mg tissue (Chandler et al. 2016a). Tissues
207 were sonicated, vortexed and incubated on ice for 30 minutes before centrifugation at 16,000 g
208 and 4 ˚C. Five µl of supernatant was injected on a Dionex Ultimate 3000 LC system coupled to
209 QExactive High Field mass spectrometer (Thermo Fisher Scientific, Waltham, MA, USA); each
210 analysis was performed with three technical replicates. Chromatographic separation was
211 achieved with Accucore HILIC chromatography (100 x 2.1 mm, 2.6 µm, 80Å; Thermo Fisher
212 Scientific, Waltham, MA, USA). Untargeted data were extracted with XCMS (Smith et al.
213 2006) and *xMSanalyzer* (Uppal et al. 2013), recovering 2,956 features (high resolution *m/z* peak
214 paired with retention time). Feature intensities were $\log_2$-transformed prior to integrative
215 network analysis using *xMWAS* (Uppal et al. 2018). The pathway enrichment analysis by

216 *mummichog* software (Li et al. 2013) was used to identify metabolic pathways enriched in mass
217 spectral features obtained from *xMWAS* analyses (Uppal et al. 2018); this approach was
218 previously validated for relevant metabolites by coelution with pure standards and MS^2 spectra
219 (Frediani et al. 2014; Uppal et al. 2017).
220
221 **Data integration and network analysis**
222 Immune cells (Cd+H1N1 significantly different from H1N1 alone), gene transcripts (from
223 leading edges of gene sets significantly different between Cd+H1N1 and H1N1 alone) and lung
224 *m/z* features (all) were selected for *xMWAS* analysis to identify Cd-dependent associations during
225 H1N1 infection. *xMWAS* (Uppal et al. 2018) uses the sparse partial least squares (sPLS)
226 regression method and the *network( )* function implemented in R package mixOmics (Gonzalez
227 et al. 2012; Le Cao et al. 2009) for generating the association matrices between datasets, with
228 Student's t-test used to evaluate the statistical significance of pairwise association scores.
229
230 **Statistics**
231 Data are presented as the mean and standard error of the mean. One-way ANOVA with Holm-
232 Sidak's post-test was used to test statistical significance at a significance level of $p < 0.05$. The
233 GSEA applet (v. 2.2; Broad Institute) produced all statistics for gene set enrichment
234 (Subramanian et al. 2005). Genes were ranked according the "Signal2Noise" statistic with a
235 significance threshold of false discovery rate (FDR)-adjusted $q < 0.05$. In *xMWAS*, $p < 0.05$ was
236 the significance threshold for correlations.
237
238
239

240 **Data Sharing**

241 In addition to Supplementary Figures, data corresponding to the Figures and Supplementary
242 Figures have been provided as numbered Supplementary Files. Datasets corresponding to
243 metabolomics and transcriptomics used for *xMWAS* analysis have also been included (see List of
244 Supplementary Files).

245

246

247

248

249

250

251

252

253

254

255

256

257

258

259

260

261

262

263

264 **Results**

265

266 **Selection of sub-lethal H1N1 dose**

267 Selection of H1N1 virus titer for mouse infection was critical to achieve maximal sub-lethal
268 morbidity as evaluated by body mass decrease and increased lung inflammation at Day 10 post-
269 infection. We compared the effects of 5 different virus doses on severity of lung infection,
270 measuring body weight change over 10 days and observing lung inflammatory histopathology at
271 Day 10 (**Supplementary Figure 1A**). The results showed that the virus doses of 0.6-1.2 x 10^3
272 pfu caused sustained body weight loss up to Day 10 post-infection. Lower doses exhibited body
273 weight recovery after Day 8 or 9. Doses of 0.6-1.2 x 10^3 pfu also caused extensive inflammatory
274 peribronchiolar histopathology (**Supplementary Figure 1B**). We reasoned that the lowest dose
275 that caused sustained body weight loss (0.6 x 10^3 pfu) would enhance the ability to detect
276 second-hit effects of Cd and selected this dose for the main study involving Cd pre-treatment
277 before infection. Consistent with previous low-dose Cd studies (Thijssen et al. 2007), Cd pre-
278 treatment had no effect on body mass or weight gain compared to vehicle treatment in the weeks
279 prior to infection (**Supplementary Figure 1C**).

280

281 **Impact of Cd treatment on pathology of H1N1 infection**

282 Four groups of mice were maintained for the treatment period, half receiving vehicle (sterile
283 drinking water) and half receiving low-dose Cd. At 10 days prior to termination, mice were
284 intranasally exposed either to mock treatment with sterile saline (Ctl, Cd groups) or 0.6 x 10^3 pfu
285 of H1N1 (H1N1, Cd+H1N1). We examined lung histopathology to determine the extent of
286 inflammation in airway (**Figure 1B**), blood vessels (**Figure 1C**) and interstitial spaces (**Figure**
287 **1D**). As expected, H1N1 infection caused inflammation to increase compared to control in all

288 compartments (H1N1: airways, $p = 0.0016$; blood vessels, $p = 0.0095$; interstitial spaces, $p =$
289 0.0127; **Figure 1B-D**). Cd treatment alone did not significantly increase histopathological
290 scoring, and combination of Cd treatment with H1N1 did not significantly increase
291 histopathology score compared to H1N1 with vehicle treatment. However, the combination of
292 Cd+H1N1 had consistently lower *p*-values compared to control than H1N1 alone, for each
293 histological compartment (Cd+H1N1: airways, $p = 2.6 \times 10^{-4}$; blood vessels, $p = 0.0011$;
294 interstitial spaces, $p = 9.8 \times 10^{-4}$; **Figure 1B-D**). Mice treated with Cd exhibited increased lung
295 Cd burden compared to vehicle treatment (**Supplementary Figure 1D**). To compare our model
296 to human lung Cd, we used the same analytical methods to measure Cd in available lung samples
297 from both smokers (S) and non-smokers (NS) (**Supplementary Figure 1D**). Cd content (pmol
298 Cd/g wet tissue, mean ± SE) in Cd-treated mouse lung tissue [Cd (n = 7), 241 ± 32; Cd+H1N1 (n
299 = 7), 220 ± 29] overlapped the range of non-smokers (n = 5, 157 ± 29) and lower portion of the
300 range for smokers (n = 14, 568 ± 137). Lung tissue Cd content in vehicle-treated mice was lower
301 than in Cd-treated mice [Ctl (n = 7), 137 ± 70; H1N1 (n = 8), 24 ± 7]. Treatment with Cd had no
302 effect on infection-mediated body weight loss (Day 10 percentage of Day 0 body weight at
303 inoculation: H1N1, 78 ± 2%; Cd+H1N1, 79 ± 2%, **Supplementary Figure 1E**), infection-
304 mediated airway enhanced paused (PenH; mean Day 10 results as percentage of Day 0 value:
305 H1N1, 700 ± 85%; Cd+H1N1, 669 ± 56%, **Supplementary Figure 1F**) or lung virus titer
306 (H1N1, 10.0 ± 0.3 $\log_{10}$[EID_{50}/ml]; Cd+H1N1, 9.6 ± 0.4 $\log_{10}$[EID_{50}/ml], **Supplementary**
307 **Figure 1G**).
308
309 **Cd increased H1N1-mediated lung tissue inflammatory cells**
310 Specific cellular contributions to lung inflammation were quantified using flow cytometry
311 (**Figure 2**). Inflammatory immune cells were increased in lung tissue of Cd+H1N1 compared to

312 H1N1, including neutrophils (p = 0.0002), monocytes (p = 0.0011), CD11b$^+$ dendritic cells
313 (DCs; p = 0.0001), CD103$^+$ DCs ($p = 3x10^{-6}$), plasmacytoid DCs (pDCs) ($p = 7x10^{-6}$), CD4$^+$ T
314 lymphocytes (p = 0.0001) and CD8$^+$ T lymphocytes (p = 0.0019) (**Figure 2A-G**). In contrast, we
315 did not observe significant differences in the numbers of lung tissue alveolar macrophages or
316 eosinophils when comparing Cd+H1N1 and H1N1 (**Supplementary Figure 2**).
317
318 **Impact of Cd on glutathione and cysteine in lung tissue and plasma**
319 We measured the steady-state redox potentials of glutathione (E_h[GSSG]) and cysteine
320 (E_h[CySS]) in plasma and lung tissue to establish whether low dose Cd treatment impacted these
321 thiol-disulfide antioxidant systems in the context of sub-lethal influenza infection. H1N1
322 treatment did cause significant oxidation of E_h[CySS] in lung tissue (**Supplementary Figure**
323 **3B**), while no effects were observed for lung glutathione or for plasma (**Supplementary Figure**
324 **3A,C-D**). No potentiation of the effect noted in lung tissue E_h[CySS] by low dose Cd was
325 observed.
326
327 **Cd enhanced pro-inflammatory gene set expression in H1N1-infected mice**
328 To determine whether Cd impacted gene expression responses to H1N1 infection, we used
329 Affymetrix MoGene ST 2.0 arrays followed by Gene Set Enrichment Analysis (GSEA)
330 (Subramanian et al. 2005) to study effects on transcript abundances among the treatment groups,
331 comparing overrepresentation of gene sets between experimental groups (n = 5). We selected
332 GSEA gene sets with $p < 0.05$ and FDR $q < 0.05$ for gene set enrichment. Seven gene sets
333 passed these criteria when comparing Cd+H1N1 and H1N1 (**Table 1**), including six that were
334 overrepresented in Cd+H1N1 compared to H1N1 alone (1. allograft rejection, 2. complement
335 signaling, 3. inflammatory response, 4. IFNα response, 5. IFNγresponse, 6. TNF-α signaling via

336 NF-κB; each comprised predominantly of pro-inflammatory genes). The seventh gene set
337 (myogenesis; comprised of cytoskeletal subunit genes) was overrepresented in H1N1 compared
338 to Cd+H1N1. Each of the six gene sets overrepresented in Cd+H1N1 compared to H1N1 was
339 also overrepresented in either of the H1N1-infected groups compared to mock-treated groups. In
340 contrast, the myogenesis gene set was overrepresented in Ctl, Cd and H1N1 groups compared to
341 Cd+H1N1.

342 The leading edge genes from each of the gene sets in **Table 1** were selected for global
343 correlation analysis by *xMWAS* (Uppal et al. 2018). After accounting for redundancies across
344 gene sets, this yielded 293 leading edge genes (**Supplementary File S3**). Two-hundred and
345 twenty of these genes belonged to the pro-inflammatory gene sets in Table 1 that were increased
346 in Cd+H1N1 compared to H1N1. Pro-inflammatory leading edge genes were predominantly
347 comprised of cytokines, chemokines, receptors of cell activation and signaling proteins. The
348 highest ranked leading edge gene from these sets (contributing most to their enrichment) was
349 'interleukin 6 (interferon, beta 2)' (*Il6*). The remaining 73 leading edge genes belonged to the
350 myogenesis gene set with cytoskeletal subunit and regulatory genes including 'actin, alpha 1'
351 (*Acta1*), 'creatine kinase, muscle' (*Ckm*) and 'collagen 1A1' (*Col1a1*). The lowest ranked gene
352 from this gene set (contributing most to the "negative enrichment" of the gene set in Cd+H1N1
353 compared to H1N1 alone; **Table 1**) was 'myosin, light chain 7, regulatory' (*Myl7*).
354

355 **Global correlation analysis of Cd effect on lung response to H1N1 influenza infection**

356 To reveal organization of the network structure and pinpoint molecules critical to Cd-altered
357 lung function, global correlations were made for immune cell counts, leading edge gene
358 transcripts and metabolites using *xMWAS* (Uppal et al. 2018). *xMWAS* is a data-driven
359 integration and network analysis tool which uses community detection to improve understanding

360 of complex interactions. As input, we used the 293 leading edge genes from Table 1 gene sets
361 (**Supplementary File S3**) paired with inflammatory cells as measured in **Figure 2A-G**
362 (**Suppelementary File S4**) and lung tissue metabolites measured by HRM (total of 2,956
363 metabolic features; **Supplementary File S5**) to produce experimental group-specific association
364 networks, with the explicit goal to compare the respective associations of the H1N1 and
365 Cd+H1N1 networks (**Figure 3**; n = 5). Student's t-test was used to determine the association
366 score (absolute value) threshold of 0.88 (determined by *xMWAS* software based on $p < 0.05$
367 criteria and n = 5 samples per group). The resulting network of H1N1 was comprised of 426
368 metabolic features, 160 gene transcripts and 7 immune cell types, while the network of
369 Cd+H1N1 was comprised of 478 metabolic features, 158 gene transcripts and 6 immune cell
370 types (**Figure 3A**; full network membership given in **Supplementary File S6**).
371 To quantify the relative importance of "nodes" (cells, transcripts or metabolites) in each
372 network, *xMWAS* calculates an eigenvector centrality score that can be compared across the
373 groups (**Figure 3B**). Respective delta centrality scores showed that monocytes (+0.419), $CD11b^+$
374 DCs (+0.380) and neutrophils (+0.301) had increased centrality in the Cd+H1N1 network
375 compared to H1N1 (**Figure 3B**). Notably, these are all myeloid cell populations, so this result
376 indicates an increase in myeloid cell importance in the Cd+H1N1 model. This result can also be
377 qualitatively detected in the model visualizations, in which neutrophils, a major myeloid cell
378 type, shift from peripheral (H1N1) to central (Cd+H1N1) network locations between the two
379 experimental conditions, whereas $CD4^+$ and $CD8^+$ T lymphocytes, canonical lymphoid cells, do
380 the opposite (**Figure 3A**). Additionally, $CD103^+$, a lymphoid dendritic cell sub-population, was
381 not found in the Cd+H1N1 network (indicating no strong correlations were made with this cell
382 type in the network (**Figure 3A**). Thus, Cd treatment altered biological interactions of immune

383 cells with gene transcript and metabolites in lung tissue following sub-lethal H1N1 infection,
384 causing myeloid cell associations to be strengthened.

385 Previous research showed that influenza-induced IFNγ restricts protective innate
386 lymphoid cell group II function in mouse lung following challenge with H1N1 (Califano et al.
387 2018). We therefore performed targeted tests to determine whether correlations with IFNγ
388 protein, measured in lung tissue homogenate by ELISA, differed for myeloid and lymphoid cells
389 in Cd+H1N1 compared to H1N1. Results showed that each myeloid cell count correlated with
390 IFNγ only in Cd+H1N1 mice [monocytes (Cd+H1N1, $r = 0.97$, $p = 3x10^{-7}$; H1N1, $r = 0.21$, $p =$
391 0.4862; **Figure 3C**), $CD11b^+$ DCs (Cd+H1N1, $r = 0.92$, $p = 2x10^{-5}$; H1N1, $r = -0.05$, p = 0.8657;
392 **Figure 3D**) and neutrophils (Cd+H1N1, $r = 0.89$, p = $9x10^{-5}$; H1N1, $r = 0.22$, $p = 0.4773$;
393 **Figure 3E**)]. Additionally, pDC exhibited a modest correlation with IFNγ in Cd+H1N1 not
394 observed in H1N1 (Cd+H1N1, $r = 0.69$, $p = 0.0122$; H1N1, $r = -0.12$, $p = 0.6869$), while none of
395 the lymphoid cell populations tested ($CD8^+$, $CD4^+$, $CD103^+$ DCs) exhibited significant
396 correlations with IFNγ in either H1N1 or Cd+H1N1 groups (**Supplementary Figure 4**). The
397 results confirm the global correlation network analysis showing that Cd burden increases
398 centrality of myeloid cells with pro-inflammatory pathways following H1N1 infection.
399 Furthermore, the strength of the IFNγ correlations in Cd+H1N1 across cell types followed the
400 same rank order as delta centrality (**Figure 3B**). These results implicate IFNγ signaling as highly
401 relevant to increased inflammation and myeloid cell dominance caused by Cd treatment.
402

403 **Gene sets and metabolic pathways associated with Cd effect on immune cell responses to**
404 **H1N1**

405 We further examined the molecular composition of each of the correlation networks to determine
406 which gene transcripts and metabolic pathways were central in each group. The overall network

407 composition of Cd+H1N1 and H1N1 overlapped by >50% in both leading edge genes and
408 metabolic features so we focused on the most divergent relationships between Cd+H1N1 and
409 H1N1 by analyzing genes and metabolites with absolute delta eigenvector
410 centrality, $|\text{Centrality}_{\text{Cd+H1N1}} - \text{Centrality}_{\text{H1N1}}|$, ≥ 0.1. (If a gene or metabolic feature was not
411 present in one of the correlation networks, its eigenvector centrality was considered 0.) Results
412 for the transcriptome data showed 83 leading edge genes of ≥ 0.1 absolute delta centrality were
413 present in the Cd+H1N1 and H1N1 networks (**Supplementary File S8**), with the IFNγ response
414 gene set (27.4% of total gene counts; **Figure 4A**) being most represented. IFNα response
415 (17.8%) followed, and myogenesis was least represented (5.2%). The IFNγ transcript, *Ifng*, had
416 differential centrality of +0.435 for Cd+H1N1 network compared to H1N1. The transcript with
417 most positive change for gene centrality (1.0) was immediate early response 2, *Ier2*, encoding a
418 DNA-binding protein, and the transcript with most negative change for gene centrality (-0.88)
419 was Dnaj (Hsp40) homolog, subfamily B, member 4, *DnajB4*, a chaperone protein targeted to the
420 plasma membrane. Thus, the transcript data are consistent with Cd effects occurring through
421 IFNγ-dependent signaling mechanisms and also involving more complex interactions of nuclear
422 as well as plasma membrane systems.
423 Prior research has shown that low-dose Cd has widespread effects on metabolism,
424 especially related to oxidative stress, mitochondrial β-oxidation of fatty acids and amino acid
425 metabolism (Go et al. 2015). We analyzed 165 metabolic features with delta eigenvector
426 centrality ≥ 0.1 (**Supplementary File S9**), using the metabolic pathway analysis software,
427 *mummichog* 1.0.10 (Li et al. 2013). The top metabolic pathway was methionine and cysteine
428 metabolism (**Figure 4B**). The largest positive centrality change for a single metabolite was for
429 S-adenosylhomocysteine (+0.415), an intermediate in methylation processes linked to
430 methionine. Other pathways included vitamin B3 (niacin/NAD), urea cycle and

431 glycerophospholipid metabolism, all of which are connected to mitochondrial function and
432 known to be perturbed by Cd. Other metabolic pathways included amino acid, pyrimidine and
433 purine pathways that have previously been associated with inflammation and/or cell proliferation
434 and turnover (**Figure 4B**). Consistent with this, the metabolite with the most negative centrality
435 change was adenine (-0.953). The results are consistent with Cd potentiation of inflammation to
436 H1N1 infection through widespread effects of low-dose Cd exposure on oxidative stress,
437 mitochondrial function and regulation of immune cell populations through IFNγ.
438
439
440
441
442
443
444
445
446
447
448
449
450
451
452
453
454

455 **Discussion**

456 A previous study showed that blood concentrations of toxic metals including Cd were
457 significantly higher in H1N1 cases with pneumonia versus pneumonia not caused by H1N1, and
458 two H1N1 cases having highest Cd concentrations did not recover from illness (Moya et al.
459 2013). Although limited by the small number of cases, the study suggested that Cd could be a
460 risk factor for inflammatory response and enhanced severity of H1N1 virus infection-induced
461 respiratory diseases. In the present study using a mouse model of H1N1 infection, we show that
462 lung Cd burden, at a value present in human lung, exacerbated inflammation and lung injury
463 from H1N1 infection in mice. Comparing Cd+H1N1 to H1N1-infected mice, Cd increased the
464 Day 10 post-infection lung burden of myeloid (monocytes, neutrophils), lymphoid ($CD4^+$ and
465 $CD8^+$ T cells) and multi-origin (DCs) bone marrow lineages of immune cells. Integrated
466 network analysis of omics data further showed that Cd burden shifted the immune response from
467 one centered on both lineages to one with myeloid cells (including $CD11b^+$ DCs) as a dominant
468 central hub. Thus, high Cd burden appears to contribute to worse outcomes following H1N1
469 infection by increasing the immune response with suppression of lymphoid and enhancement of
470 myeloid cell participation in response to infection.

471 The global correlation network analysis of immune cells with gene transcript and
472 metabolite abundances revealed the centrality of myeloid cells (monocytes, $CD11b^+$ DCs
473 [considered a myeloid DC subtype (Chistiakov et al. 2015)] and neutrophils) in the Cd+H1N1
474 group. Transcriptional responses suggest that Cd primes myeloid cells for tight coordination
475 with IFNγ signaling. The finding that a unique lysosomal thiol reductase, IFNγ-inducible
476 lysosomal thiol reductase, controls conditions for degradation of proteins to small peptides in
477 lysosomes (Hastings and Cresswell 2011; Phan et al. 2002), raises the possibility that Cd
478 specifically impacts IFNγ-dependent functions through interaction with, or oxidation of, the

479 thioredoxin-like active site involved in disulfide reduction. Low dose Cd causes oxidation and
480 disruption of the actin-cytoskeleton (Go et al. 2013a), suggesting that targeted effects on a
481 critical signaling system could occur even without effects on major GSH or thioredoxin systems.
482 Effects of low-dose Cd on the actin-cytoskeleton system triggers translocation of Trx1 to cell
483 nuclei (Go et al. 2013a) and increase NF-κB activation (Go et al. 2011; Go et al. 2013b) and
484 monocyte adhesion (Go and Jones 2005). Thus, these processes also could contribute to higher
485 immune cell counts in Cd+H1N1 compared to H1N1. The GSEA results showing effects of Cd
486 on pro-inflammatory gene sets (**Table 1**), as well as increased cytokine levels and immune cell
487 counts, support such a Cd-dependent mechanism.
488 Alternative mechanisms for Cd effects on inflammatory pathology of H1N1 could
489 involve cytoskeletal functions, myogenesis and elastogenesis in the inflamed and injured lungs.
490 It is noteworthy that the combination of Cd pre-treatment with H1N1 infection was the
491 experimental condition to cause a significant negative enrichment, or decrease in overall
492 transcript levels, of the myogenesis gene set. Cytoskeletal regulation by tight junctions and
493 adherens junctions is a key element of airway permeability to infiltrating immune cells (Rezaee
494 and Georas 2014). We previously found that low dose Cd disruption of actin cytoskeleton
495 regulation (Go et al. 2013a; Hu et al. 2017) triggered nuclear translocation of thioredoxin-1 and
496 caused cell death (Go et al. 2013b). A study by Desouza *et al*. also showed that actin-binding
497 proteins contribute to cell death, and actin dynamics plays a key role in regulating apoptosis
498 signaling (Desouza et al. 2012). Studies of low dose Cd effects on actin cytoskeleton and cell
499 death in fibroblasts, HeLa and HT-29 cells [(Go et al. 2013a; Hu et al. 2017); Y.-M. Go, D.P.
500 Jones, unpublished] suggest that this could be a general cell response and contribute to barrier
501 dysfunction. Thus, Cd could also contribute to severity of response through mechanisms

502 involving impaired myogenesis, elastogenesis, increased cell death and failure to clear cell debris
503 in the inflamed and injured lungs.

504 In contrast to the coherent picture provided by Cd effects on proinflammatory signaling,
505 immune cell accumulation in the lungs and amplified effects on myeloid compared to lymphoid
506 cells, metabolic effects associated with Cd effects were diverse and complex; the results
507 suggested more of a generalized adaptive response than a causal role in exacerbation of
508 inflammation. The top pathway from pathway enrichment analysis was for sulfur-containing
509 amino acids which serve to support GSH synthesis and antioxidant activities. This would appear
510 to be a protective mechanism, but maladaptive effects could also occur at specific subcellular
511 sites. Pathway enrichment analysis also showed that pathways of several amino acids,
512 nucleosides and phospholipids were overrepresented in the networks with differential
513 eigenvector centrality ≥ 0.1 (**Figure 4B**). Overall, these results suggest that Cd burden causes a
514 complex array of metabolic responses.

515 Inhaled Cd causes acute pneumonitis and lung edema (Nemery 1990), and intraperitoneal
516 injection of Cd causes lung inflammation in rats (Kataranovski et al. 2009). However, chronic
517 ingestion of Cd at levels mimicking those derived from the human diet has not previously been
518 directly linked to inflammatory lung disease. The present research with 16 weeks of Cd in
519 drinking water showed little evidence for inflammation without the second stimulus of H1N1
520 infection. Thus, Cd accumulation with advanced age (> 65 y), tobacco use, metabolic syndrome
521 and/or obesity, may create a sub-clinical state poised to over-react to influenza virus infection-
522 induced inflammation, which may in turn lead to worse morbidity or mortality (Choi et al. 2014;
523 Fiore et al. 2011; Lee and Kim 2016; Olsson et al. 2002; Ramsey and Kumar 2013). For future
524 research, the dose of virus used in our study permits recovery to study later complications such
525 as fibrosis caused by low-dose Cd (Hu et al. 2017).

526 Finally, in light of common consumption of foods with relatively high Cd content
527 (potatoes, cereals), the results indicate that studies in humans are needed to evaluate whether Cd
528 burden is associated with severity of response to influenza infection. Cd burden can be readily
529 evaluated by determination of Cd/creatinine level in urine (Haddam et al. 2011; Larsson and
530 Wolk 2016). While there are no approved strategies to prevent Cd accumulation or decrease its
531 burden, mechanisms discussed above could be targeted to prevent Cd-dependent potentiation of
532 influenza severity. For instance, the mechanism for nuclear Trx1 translocation could be targeted
533 to block excessive activation of transcriptional responses. Alternatively, Txnip, a vitamin D_3-
534 binding protein that controls nuclear Trx1 activity (Wang et al. 2002; Yamawaki et al. 2005),
535 could provide a target for therapeutic manipulation. Trp14 catalyzes reduction of cystine
536 (oxidized form of cysteine) (Pader et al. 2014) and could provide a target to protect against
537 oxidation of proteins and downstream signaling and recruitment of immune cells. Cd also
538 interacts with trace elements including selenium, zinc and iron (Gocmen et al. 2000; Riederer et
539 al. 2013), providing additional strategies for supplement use (Choi et al. 2014; Moya et al. 2013).
540 In summary, this study showed that mice given Cd at a level achieved in humans from
541 dietary intake had worse lung inflammation and inflammatory pathology after H1N1 influenza
542 infection, in association with enhanced myeloid-dominant pro-inflammatory gene and metabolic
543 responses. Studies are needed to evaluate whether Cd burden contributes to influenza severity in
544 humans. Combined analyses of phenotypic measures with transcriptome and metabolome
545 analyses enable global surveillance of complex systems responses to identify candidate
546 mechanisms and potential therapeutic targets.
547
548
549

550 **List of Supplementary Figures and Data Files**

551 **Supplementary Figure 1.** Virus dose response, response to Cd pre-treatment, and body mass,
552 PenH and virus titer endpoints of main study.

553 **Supplementary Figure 2.** Flow cytometry-quantified eosinophils and alveolar macrophages.

554 **Supplementary Figure 3.** Steady-state redox potentials of glutathione and cysteine in lung
555 tissue and plasma.

556 **Supplementary Figure 4.** Correlations of additional cell types with IFNγ.

557 **Supplementary File S1.** Corresponds to Figure 1 histopathology data.

558 **Supplementary File S2.** Corresponds to Figure 2 flow cytometry data.

559 **Supplementary File S3.** Leading edge genes selected for *xMWAS* analysis.

560 **Supplementary File S4.** Flow cytometry results selected for *xMWAS* analysis.

561 **Supplementary File S5.** Metabolomics dataset selected for *xMWAS* analysis.

562 **Supplementary File S6.** Corresponds to Figure 3 *xMWAS* analysis data and IFNγ correlations.

563 **Supplementary File S7.** Corresponds to Figure 4 enrichment tests data.

564 **Supplementary File S8.** Leading edge genes used for proportion testing following *xMWAS*.

565 **Supplementary File S9.** Metabolite features used for *mummichog* testing following *xMWAS*.

566 **Supplementary File S10.** Full Robust Multi-Array dataset from lung tissue Affymetrix array.

567 **Supplementary File S11.** Corresponds to Figure S1 data.

568 **Supplementary File S12.** Corresponds to Figure S2 data.

569 **Supplementary File S13.** Corresponds to Figure S3 data.

570 **Supplementary File S14.** Corresponds to Figure S4 data.

571

572

573

574 **References**

575 Baigent SJ, McCauley JW. 2003a. Influenza type a in humans, mammals and birds:
576 Determinants of virus virulence, host-range and interspecies transmission. Bioessays
577 25:657-671.
578 Baigent SJ, McCauley JW. 2003b. Influenza type a in humans, mammals and birds:
579 Determinants of virus virulence, host-range and interspecies transmission. Bioessays
580 25:657-671.
581 Bermejo-Martin JF, Ortiz de Lejarazu R, Pumarola T, Rello J, Almansa R, Ramirez P, et al.
582 2009. Th1 and th17 hypercytokinemia as early host response signature in severe
583 pandemic influenza. Crit Care 13:R201.
584 Califano D, Furuya Y, Roberts S, Avram D, McKenzie ANJ, Metzger DW. 2018. Ifn-gamma
585 increases susceptibility to influenza a infection through suppression of group ii innate
586 lymphoid cells. Mucosal Immunol 11:209-219.
587 Chandler JD, Hu X, Ko EJ, Park S, Lee YT, Orr M, et al. 2016a. Metabolic pathways of lung
588 inflammation revealed by high-resolution metabolomics (hrm) of h1n1 influenza virus
589 infection in mice. Am J Physiol Regul Integr Comp Physiol 311:R906-R916.
590 Chandler JD, Wongtrakool C, Banton SA, Li S, Orr ML, Barr DB, et al. 2016b. Low-dose oral
591 cadmium increases airway reactivity and lung neuronal gene expression in mice. Physiol
592 Rep 4.
593 Chistiakov DA, Sobenin IA, Orekhov AN, Bobryshev YV. 2015. Myeloid dendritic cells:
594 Development, functions, and role in atherosclerotic inflammation. Immunobiology
595 220:833-844.
596 Choi SM, Jeong YJ, Park JS, Kang HJ, Lee YJ, Park SS, et al. 2014. The impact of lifestyle
597 behaviors on the acquisition of pandemic (h1n1) influenza infection: A case-control
598 study. Yonsei Med J 55:422-427.
599 Desouza M, Gunning PW, Stehn JR. 2012. The actin cytoskeleton as a sensor and mediator of
600 apoptosis. Bioarchitecture 2:75-87.
601 Fiore AE, Fry A, Shay D, Gubareva L, Bresee JS, Uyeki TM. 2011. Antiviral agents for the
602 treatment and chemoprophylaxis of influenza --- recommendations of the advisory
603 committee on immunization practices (acip). MMWR Recomm Rep 60:1-24.

604 Frediani JK, Jones DP, Tukvadze N, Uppal K, Sanikidze E, Kipiani M, et al. 2014. Plasma
605 metabolomics in human pulmonary tuberculosis disease: A pilot study. PLoS One
606 9:e108854.
607 Gagnon A, Miller MS, Hallman SA, Bourbeau R, Herring DA, Earn DJ, et al. 2013. Age-specific
608 mortality during the 1918 influenza pandemic: Unravelling the mystery of high young
609 adult mortality. PLoS One 8:e69586.
610 Gautam M. 2012. Endothelial cells as regulators of cytokine storms during influenza infection.
611 Thorax 67:617-617.
612 Go YM, Jones DP. 2005. Intracellular proatherogenic events and cell adhesion modulated by
613 extracellular thiol/disulfide redox state. Circulation 111:2973-2980.
614 Go YM, Jones DP. 2011. Cysteine/cystine redox signaling in cardiovascular disease. Free Radic
615 Biol Med 50:495-509.
616 Go YM, Kang SM, Roede JR, Orr M, Jones DP. 2011. Increased inflammatory signaling and
617 lethality of influenza h1n1 by nuclear thioredoxin-1. PLoS One 6:e18918.
618 Go YM, Orr M, Jones DP. 2013a. Actin cytoskeleton redox proteome oxidation by cadmium.
619 Am J Physiol Lung Cell Mol Physiol 305:L831-843.
620 Go YM, Orr M, Jones DP. 2013b. Increased nuclear thioredoxin-1 potentiates cadmium-induced
621 cytotoxicity. Toxicological sciences 131:84-94.
622 Go YM, Roede JR, Orr M, Liang Y, Jones DP. 2014. Integrated redox proteomics and
623 metabolomics of mitochondria to identify mechanisms of cd toxicity. Toxicological
624 sciences 139:59-73.
625 Go YM, Sutliff RL, Chandler JD, Khalidur R, Kang BY, Anania FA, et al. 2015. Low-dose
626 cadmium causes metabolic and genetic dysregulation associated with fatty liver disease
627 in mice. Toxicological sciences 147:524-534.
628 Gocmen C, Kumcu EK, Secilmis A, Ucar P, Dikmen A, Baysal F. 2000. Restorative effects of
629 zinc and selenium on nitrergic relaxations impaired by cadmium in the mouse corpus
630 cavernosum. Toxicol Lett 111:229-234.
631 Gonzalez I, Cao KA, Davis MJ, Dejean S. 2012. Visualising associations between paired 'omics'
632 data sets. BioData Min 5:19.
633 Haddam N, Samira S, Dumont X, Taleb A, Lison D, Haufroid V, et al. 2011. Confounders in the
634 assessment of the renal effects associated with low-level urinary cadmium: An analysis in
635 industrial workers. Environ Health 10:37.

636 Hastings KT, Cresswell P. 2011. Disulfide reduction in the endocytic pathway: Immunological
637 functions of gamma-interferon-inducible lysosomal thiol reductase. Antioxid Redox
638 Signal 15:657-668.
639 Horby P, Nguyen NY, Dunstan SJ, Baillie JK. 2012. The role of host genetics in susceptibility to
640 influenza: A systematic review. PLoS One 7:e33180.
641 Horby P, Nguyen NY, Dunstan SJ, Baillie JK. 2013. An updated systematic review of the role of
642 host genetics in susceptibility to influenza. Influenza Other Respir Viruses 7 Suppl 2:37-
643 41.
644 Hu X, Fernandes J, Jones DP, Go YM. 2017. Cadmium stimulates myofibroblast differentiation
645 and mouse lung fibrosis. Toxicology 383:50-56.
646 Hwang HS, Lee YT, Kim KH, Park S, Kwon YM, Lee Y, et al. 2016. Combined virus-like
647 particle and fusion protein-encoding DNA vaccination of cotton rats induces protection
648 against respiratory syncytial virus without causing vaccine-enhanced disease. Virology
649 494:215-224.
650 Jones DP, Mody VC, Jr., Carlson JL, Lynn MJ, Sternberg P, Jr. 2002. Redox analysis of human
651 plasma allows separation of pro-oxidant events of aging from decline in antioxidant
652 defenses. Free Radic Biol Med 33:1290-1300.
653 Jones DP, Liang Y. 2009. Measuring the poise of thiol/disulfide couples in vivo. Free Radic Biol
654 Med 47:1329-1338.
655 Kataranovski M, Mirkov I, Belij S, Nikolic M, Zolotarevski L, Ciric D, et al. 2009. Lungs:
656 Remote inflammatory target of systemic cadmium administration in rats. Environ Toxicol
657 Pharmacol 28:225-231.
658 Ko EJ, Lee YT, Kim KH, Jung YJ, Lee Y, Denning TL, et al. 2016. Effects of mf59 adjuvant on
659 induction of isotype-switched igg antibodies and protection after immunization with t-
660 dependent influenza virus vaccine in the absence of cd4+ t cells. J Virol 90:6976-6988.
661 Larsson SC, Wolk A. 2016. Urinary cadmium and mortality from all causes, cancer and
662 cardiovascular disease in the general population: Systematic review and meta-analysis of
663 cohort studies. Int J Epidemiol 45:782-791.
664 Le Cao KA, Gonzalez I, Dejean S. 2009. Integromics: An r package to unravel relationships
665 between two omics datasets. Bioinformatics 25:2855-2856.

666 Lee BK, Kim Y. 2016. Association of blood cadmium level with metabolic syndrome after
667 adjustment for confounding by serum ferritin and other factors: 2008-2012 korean
668 national health and nutrition examination survey. Biol Trace Elem Res 171:6-16.
669 Lee YN, Kim MC, Lee YT, Kim YJ, Lee J, Kim C, et al. 2015. Co-immunization with tandem
670 repeat heterologous m2 extracellular proteins overcomes strain-specific protection of split
671 vaccine against influenza a virus. Antiviral Res 122:82-90.
672 Lee YT, Ko EJ, Lee Y, Lee YN, Bian Z, Liu Y, et al. 2016. Cd47 plays a role as a negative
673 regulator in inducing protective immune responses to vaccination against influenza virus.
674 J Virol 90:6746-6758.
675 Li S, Park Y, Duraisingham S, Strobel FH, Khan N, Soltow QA, et al. 2013. Predicting network
676 activity from high throughput metabolomics. PLoS Comput Biol 9:e1003123.
677 Liu M, Zhao X, Hua S, Du X, Peng Y, Li X, et al. 2015. Antigenic patterns and evolution of the
678 human influenza a (h1n1) virus. Sci Rep 5:14171.
679 Liu Q, Zhou YH, Yang ZQ. 2016. The cytokine storm of severe influenza and development of
680 immunomodulatory therapy. Cell Mol Immunol 13:3-10.
681 Monsalvo AC, Batalle JP, Lopez MF, Krause JC, Klemenc J, Hernandez JZ, et al. 2011. Severe
682 pandemic 2009 h1n1 influenza disease due to pathogenic immune complexes. Nat Med
683 17:195-199.
684 Moya M, Bautista EG, Velazquez-Gonzalez A, Vazquez-Gutierrez F, Tzintzun G, Garcia-
685 Arreola ME, et al. 2013. Potentially-toxic and essential elements profile of ah1n1 patients
686 in mexico city. Sci Rep 3:1284.
687 Nemery B. 1990. Metal toxicity and the respiratory tract. Eur Respir J 3:202-219.
688 Olsson IM, Bensryd I, Lundh T, Ottosson H, Skerfving S, Oskarsson A. 2002. Cadmium in
689 blood and urine--impact of sex, age, dietary intake, iron status, and former smoking--
690 association of renal effects. Environ Health Perspect 110:1185-1190.
691 Olszowski T, Baranowska-Bosiacka I, Gutowska I, Chlubek D. 2012. Pro-inflammatory
692 properties of cadmium. Acta Biochim Pol 59:475-482.
693 Pader I, Sengupta R, Cebula M, Xu J, Lundberg JO, Holmgren A, et al. 2014. Thioredoxin-
694 related protein of 14 kda is an efficient l-cystine reductase and s-denitrosylase. Proc Natl
695 Acad Sci U S A 111:6964-6969.

696 Phan UT, Lackman RL, Cresswell P. 2002. Role of the c-terminal propeptide in the activity and
697 maturation of gamma -interferon-inducible lysosomal thiol reductase (gilt). Proc Natl
698 Acad Sci U S A 99:12298-12303.
699 Ramsey CD, Kumar A. 2013. Influenza and endemic viral pneumonia. Crit Care Clin 29:1069-
700 1086.
701 Rezaee F, Georas SN. 2014. Breaking barriers. New insights into airway epithelial barrier
702 function in health and disease. Am J Respir Cell Mol Biol 50:857-869.
703 Riederer AM, Belova A, George BJ, Anastas PT. 2013. Urinary cadmium in the 1999-2008 u.S.
704 National health and nutrition examination survey (nhanes). Environ Sci Technol 47:1137-
705 1147.
706 Safronetz D, Rockx B, Feldmann F, Belisle SE, Palermo RE, Brining D, et al. 2011a. Pandemic
707 swine-origin h1n1 influenza a virus isolates show heterogeneous virulence in macaques. J
708 Virol 85:1214-1223.
709 Safronetz D, Rockx B, Feldmann F, Belisle SE, Palermo RE, Brining D, et al. 2011b. Pandemic
710 swine-origin h1n1 influenza a virus isolates show heterogeneous virulence in macaques. J
711 Virol 85:1214-1223.
712 Satarug S, Moore MR. 2004. Adverse health effects of chronic exposure to low-level cadmium
713 in foodstuffs and cigarette smoke. Environ Health Perspect 112:1099-1103.
714 Smith CA, Want EJ, O'Maille G, Abagyan R, Siuzdak G. 2006. Xcms: Processing mass
715 spectrometry data for metabolite profiling using nonlinear peak alignment, matching, and
716 identification. Anal Chem 78:779-787.
717 Subramanian A, Tamayo P, Mootha VK, Mukherjee S, Ebert BL, Gillette MA, et al. 2005. Gene
718 set enrichment analysis: A knowledge-based approach for interpreting genome-wide
719 expression profiles. Proc Natl Acad Sci U S A 102:15545-15550.
720 Suwazono Y, Kido T, Nakagawa H, Nishijo M, Honda R, Kobayashi E, et al. 2009. Biological
721 half-life of cadmium in the urine of inhabitants after cessation of cadmium exposure.
722 Biomarkers 14:77-81.
723 Taubenberger JK, Kash JC. 2010a. Influenza virus evolution, host adaptation, and pandemic
724 formation. Cell Host Microbe 7:440-451.
725 Taubenberger JK, Kash JC. 2010b. Influenza virus evolution, host adaptation, and pandemic
726 formation. Cell Host Microbe 7:440-451.

727 Thijssen S, Maringwa J, Faes C, Lambrichts I, Van Kerkhove E. 2007. Chronic exposure of mice
728 to environmentally relevant, low doses of cadmium leads to early renal damage, not
729 predicted by blood or urine cadmium levels. Toxicology 229:145-156.
730 To KK, Hung IF, Li IW, Lee KL, Koo CK, Yan WW, et al. 2010. Delayed clearance of viral
731 load and marked cytokine activation in severe cases of pandemic h1n1 2009 influenza
732 virus infection. Clin Infect Dis 50:850-859.
733 Uppal K, Soltow QA, Strobel FH, Pittard WS, Gernert KM, Yu T, et al. 2013. Xmsanalyzer:
734 Automated pipeline for improved feature detection and downstream analysis of large-
735 scale, non-targeted metabolomics data. BMC Bioinformatics 14:15.
736 Uppal K, Walker DI, Jones DP. 2017. Xmsannotator: An r package for network-based annotation
737 of high-resolution metabolomics data. Anal Chem 89:1063-1067.
738 Uppal K, Ma C, Go YM, Jones DP, Wren J. 2018. Xmwas: A data-driven integration and
739 differential network analysis tool. Bioinformatics 34:701-702.
740 Waalkes MP. 2003. Cadmium carcinogenesis. Mutat Res 533:107-120.
741 Wang Y, De Keulenaer GW, Lee RT. 2002. Vitamin d(3)-up-regulated protein-1 is a stress-
742 responsive gene that regulates cardiomyocyte viability through interaction with
743 thioredoxin. J Biol Chem 277:26496-26500.
744 Wilson N, Oliver J, Rice G, Summers JA, Baker MG, Waller M, et al. 2014. Age-specific
745 mortality during the 1918-19 influenza pandemic and possible relationship to the 1889-92
746 influenza pandemic. J Infect Dis 210:993-995.
747 Xing ZH, Sun X, Xu L, Wu Q, Li L, Wu XJ, et al. 2015. Thin-section computed tomography
748 detects long-term pulmonary sequelae 3 years after novel influenza a virus-associated
749 pneumonia. Chin Med J (Engl) 128:902-908.
750 Yamawaki H, Pan S, Lee RT, Berk BC. 2005. Fluid shear stress inhibits vascular inflammation
751 by decreasing thioredoxin-interacting protein in endothelial cells. J Clin Invest 115:733-
752 738.
753 Zhang W, Zhi J, Cui Y, Zhang F, Habyarimana A, Cambier C, et al. 2014. Potentiated interaction
754 between ineffective doses of budesonide and formoterol to control the inhaled cadmium-
755 induced up-regulation of metalloproteinases and acute pulmonary inflammation in rats.
756 PLoS One 9:e109136.
757
758

759 **Figure Legends**

760

761 **Figure 1.** Impact of low-dose Cd on H1N1 infection lung histopathology. Mice were given ad
762 libitum drinking water without or with $CdCl_2$ (1 mg/l) for 16 weeks; ten days prior to
763 completion, mice in both groups were given one intranasal dose of either sterile saline (Ctl, Cd)
764 or H1N1 influenza virus (H1N1, Cd+H1N1). Lung tissue was collected and formalin-fixed upon
765 sacrifice at Day 10 after infection. **(A)** Representative images of hematoxylin and eosin-stained
766 sections of lung tissue are shown for each group (scale bar: 100 µm). **(B)** Airway, **(C)** blood
767 vessel and **(D)** interstitial spaces were assessed for inflammatory foci in blinded fashion. n = 4-5
768 mice per group. *$p < 0.05$ compared to Ctl.

769

770 **Figure 2.** Cd increased lung immune cell response to H1N1 infection. Cells were isolated from
771 lung tissue homogenates, labeled with appropriate antibodies for **(A)** neutrophils (PMNs), **(B)**
772 monocytes, **(C)** $CD11b^+$ dendritic cells (DCs), **(D)** $CD103^+$ DCs, **(E)** plasmacytoid DCs (pDCs),
773 **(F)** $CD4^+$ T cells, **(G)** $CD8^+$ T cells and quantified by flow cytometry. Bar plots show mean ±
774 SEM of cell counts (n = 11-13, except for $CD4^+$ and $CD8^+$ T cells, n = 7-8). *$p < 0.05$ compared
775 to Ctl, #$p < 0.05$ compared to H1N1 by one-way ANOVA with Holm-Sidak's post-test.

776

777 **Figure 3.** Cd promotes mouse lung myeloid cell responses to H1N1 infection. Inflammatory
778 lung tissue cell counts (7 cell types, **Fig. 2**), leading edge gene intensities (293 leading edge
779 genes selected by GSEA, **Supplementary File 3**;) and lung tissue metabolites measured by
780 untargeted LC-MS (total of 2956 metabolic features, **Supplementary File 5**) were correlated
781 using sparse PLS regression implemented by *xMWAS* (n = 5/group). **(A)** Networks were
782 constructed of variables with inter-dataset absolute association score >0.88 at $p < 0.05$ (n = 5) for

783 H1N1 or Cd+H1N1 groups. Symbols depict metabolic features (orange rectangle), gene
784 transcripts (green circle) or cell counts (blue triangle), and lines indicate relationship between
785 symbols (red, positive correlation; blue, negative correlation). The blue triangles have been
786 enlarged for easier viewing. Abbreviations for cells are as follows: Monocytes, 'Mono';
787 neutrophils, 'PMN'; $CD11b^+$ dendritic cells, '$CD11b^+$ DC'; $CD103^+$ dendritic cells, '$CD103^+$
788 DC'; plasmacytoid dendritic cells, 'pDC'; CD4 T lymphocytes, '$CD4^+$'; and CD8 T
789 lymphocytes, '$CD8^+$'. Note, $CD103^+$ DC is not found in the Cd+H1N1 network. **(B)** The
790 absolute value of difference in eigenvector centrality (Delta Centrality) of each immune cell type
791 was contrasted between the networks of Cd+H1N1 and H1N1 networks. Pearson's correlation
792 (r) was analyzed for the abundance of lung IFNγ protein and lung monocytes **(C)**, $CD11b^+$ DCs
793 **(D)** and neutrophils **(E)**. Open circles, H1N1 alone; closed circles, Cd+H1N1. The resulting
794 statistics of correlation (r) and significance (p) were as follows: **C**, monocytes (Cd+H1N1, r =
795 0.97, $p = 3\text{x}10^{-7}$; H1N1, $r = 0.21$, $p = 0.49$); **D**, $CD11b^+$ DCs (Cd+H1N1, $r = 0.92$, $p = 2\text{x}10^{-5}$;
796 H1N1, $r = -0.05$, $p = 0.86$); **E**, neutrophils (Cd+H1N1, $r = 0.89$, $p = 9\text{x}10^{-5}$; H1N1, $r = 0.22$, p =
797 0.48). n = 12-13.
798
799 **Figure 4.** Cd potentiation of immune response to H1N1 infection through widespread effects of
800 low Cd exposure on inflammation, mitochondrial function and regulation of immune cell
801 populations through IFNγ. **(A)** Percentage of gene sets represented in the 83 leading edge genes
802 (**Supplementary Table 2**) with delta eigenvector centrality (absolute value), $|\text{Centrality}_{\text{Cd+H1N1}} -$
803 $\text{Centrality}_{\text{H1N1}}|$, ≥ 0.1 between Cd+H1N1 and H1N1 networks. **(B)** Metabolic pathway
804 enrichment analysis was performed on 165 metabolic features with delta eigenvector centrality ≥
805 0.1 between networks of Cd+H1N1 and H1N1 using *mummichog*. The negative $\log_{10}$ of the

806 pathway *p*-value is plotted as a bar graph for each significant pathway ($p < 0.05$, at least 3
807 metabolite matches in pathway).
808
809
810
811
812
813
814
815
816
817
818
819
820
821
822
823
824
825
826
827
828
829
830

831 **Table 1.** Cd increases pro-inflammatory gene enrichment in response to H1N1 challenge.

Gene Sets		**Enrichment**		
Name	Number of Genes	*H1N1 vs. Ctl*	*Cd+H1N1 vs. Ctl*	*Cd+H1N1 vs. H1N1*
Allograft rejection	189	3.02	3.21	2.31
Complement	181	2.36	2.56	1.73
Inflammatory response	199	2.61	2.75	1.84
Interferon-α response	89	2.79	2.88	2.04
Interferon-γ response	195	3.09	3.36	2.49
TNF-α signaling via NF-κB	196	2.60	2.82	2.06
Myogenesis	195	NA	-1.66	-2.14

832

833 Gene set normalized enrichment scores that are statistically significant comparing Cd+H1N1 and H1N1
834 ($p < 0.05$ and FDR $q < 0.05$) are shown. Normalized enrichment scores compared to controls (also $p <$
835 0.05 and FDR $q < 0.05$) are shown for H1N1 alone or Cd+H1N1. Negative enrichment values indicate
836 *lower* gene abundances compared to the reference group (Ctl or H1N1, indicated in the column header).
837 NA, gene set enrichment did not pass significance testing threshold.

838

839

840 **Figure 1**

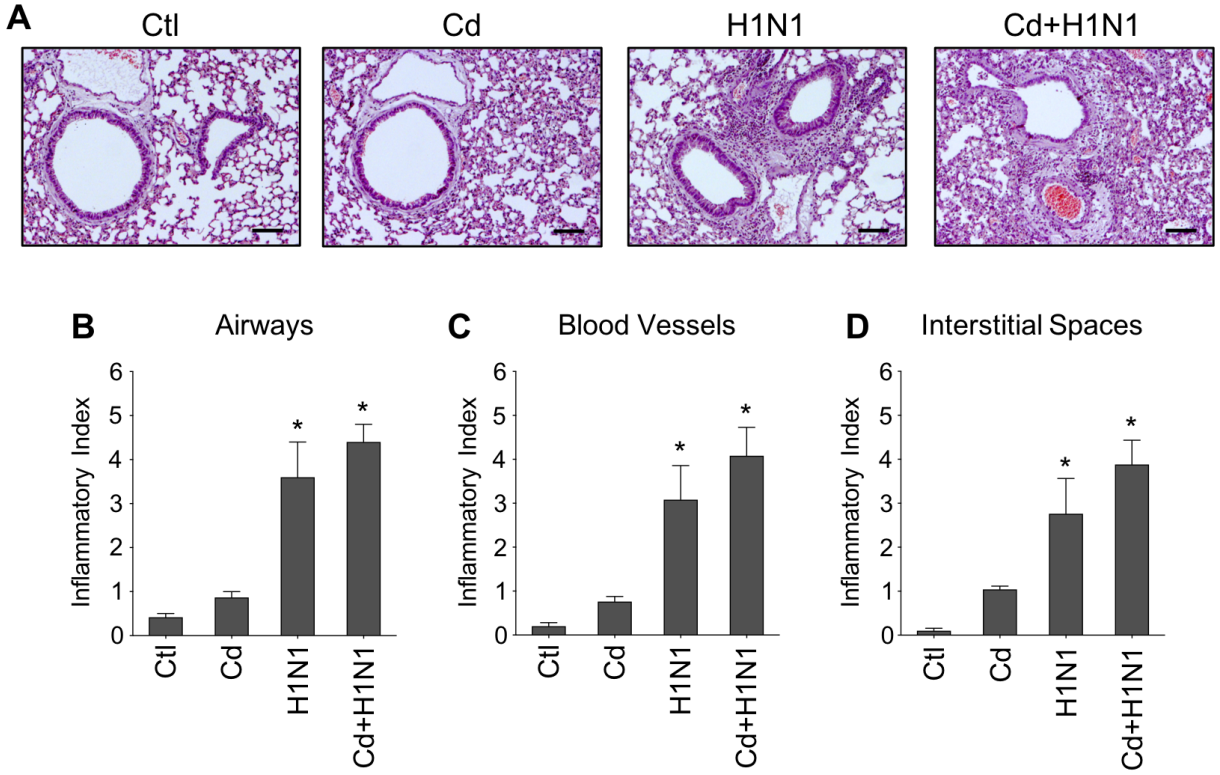

841

842

843

844

845

846

847

848

849

850

851

852

853 **Figure 2**

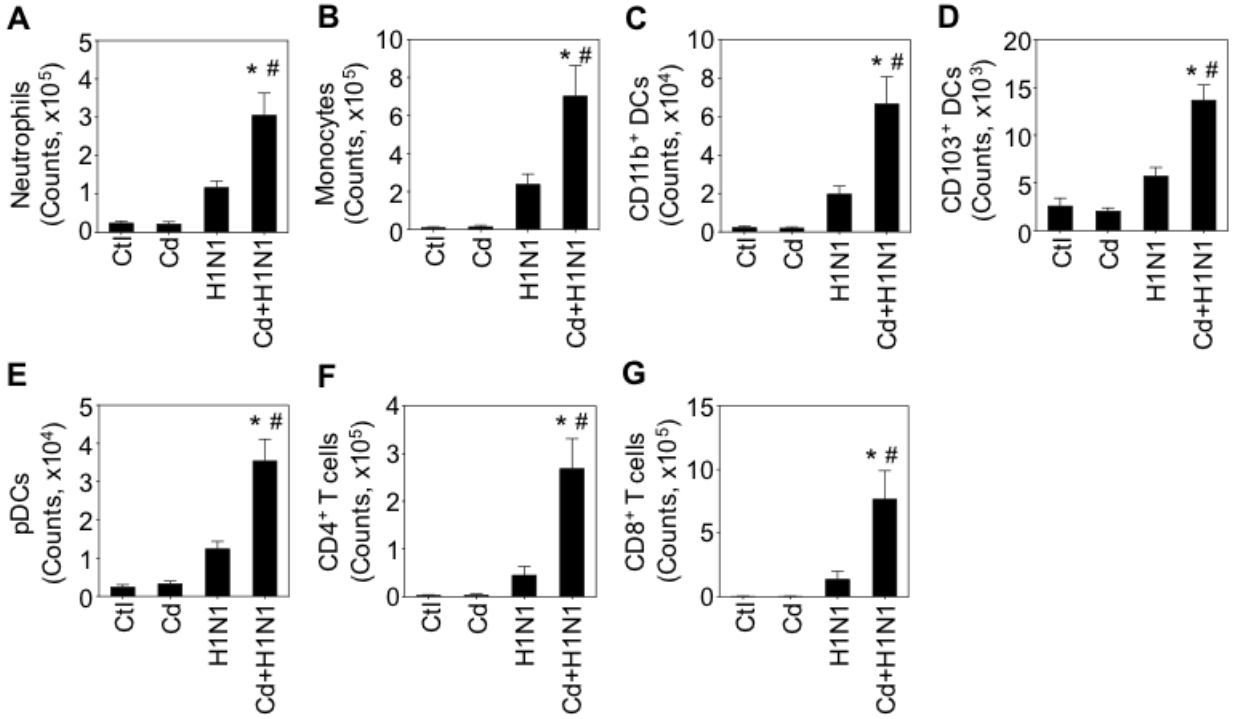

854

855

856

857

858

859

860

861

862

863

864

865

866

867 **Figure 3**

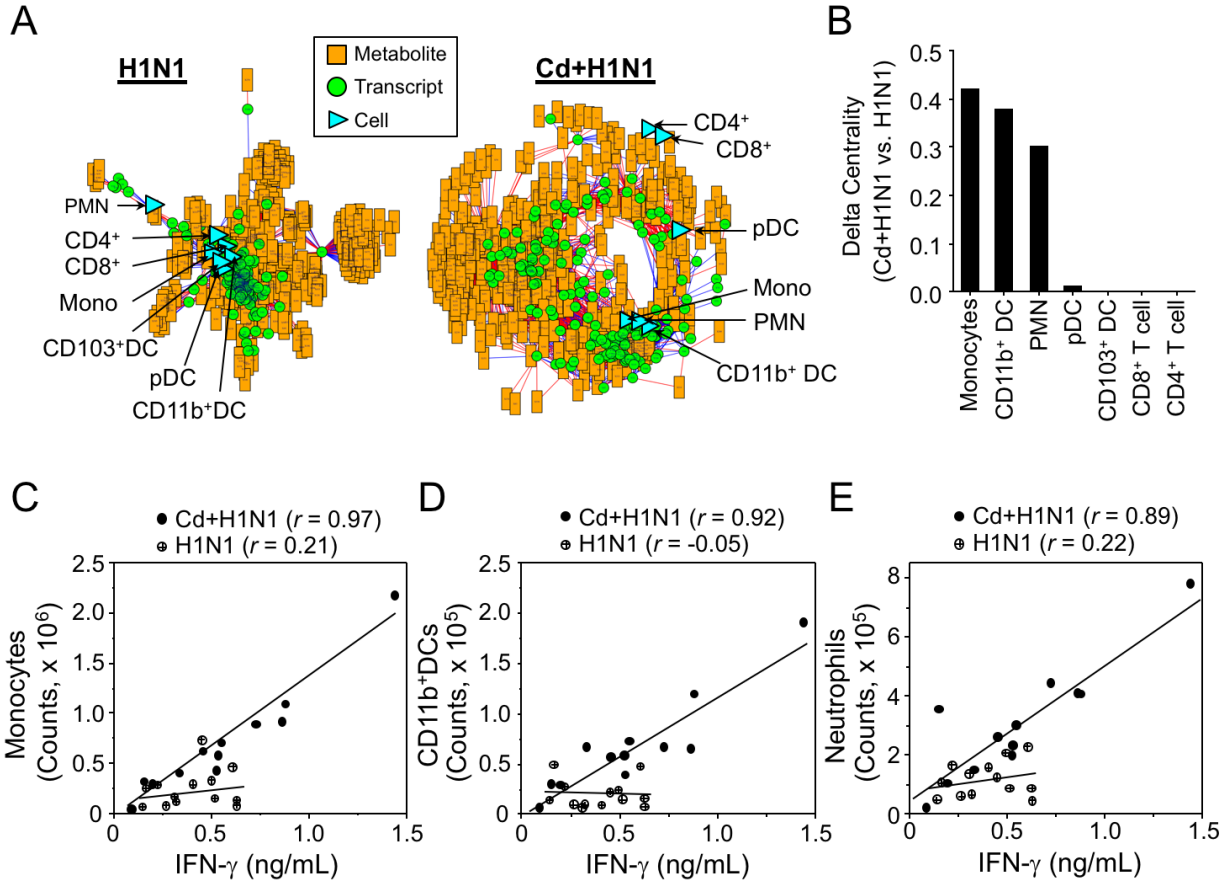

868

869

870

871

872

873

874

875

876

877

878

879 **Figure 4**

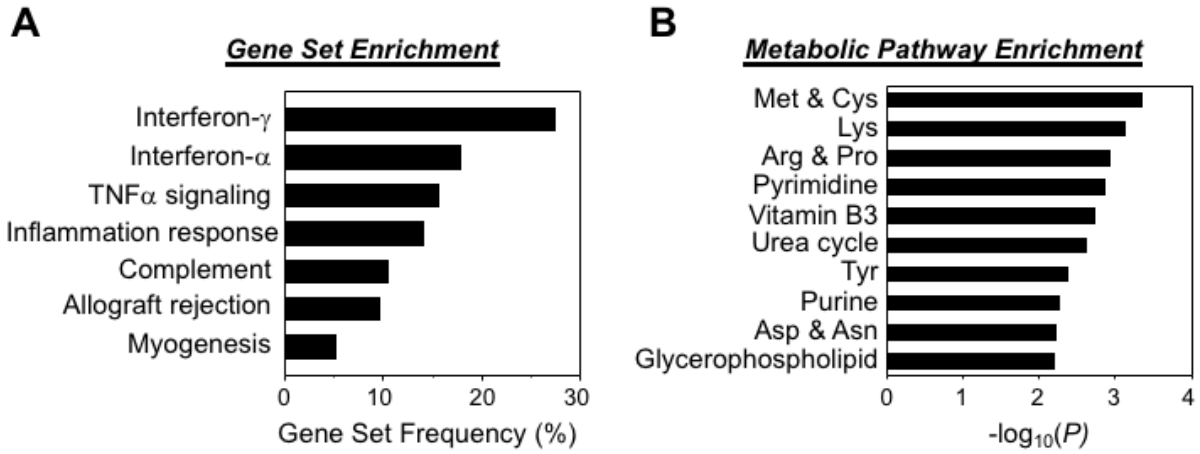

880